Journal of Power Sources 244 (2013) 158–163

Contents lists available at SciVerse ScienceDirect

Journal of Power Sources

journal homepage: www.elsevier.com/locate/jpowsour

# Real-time investigation of the structural evolution of electrodes in a commercial lithium-ion battery containing a V-added $LiFePO_4$ cathode using *in-situ* neutron powder diffraction

Chih-Wei Hu [a,b], Neeraj Sharma [c,1], Ching-Yu Chiang [b,d], Hui-Chia Su [b,*], Vanessa K. Peterson [c], Han-Wei Hsieh [e], Yu-Fang Lin [e], Wu-Ching Chou [d], Bor-Yuan Shew [b], Chih-Hao Lee [a,b]

[a] Department of Engineering and System Science, National Tsing Hua University, Hsinchu 30013, Taiwan
[b] National Synchrotron Radiation Research Center, 101 Hsin-Ann Road, Hsinchu Science Park, Hsinchu 30076, Taiwan
[c] Australian Nuclear Science and Technology Organisation, Locked Bag 2001, Kirrawee DC, NSW 2232, Australia
[d] Institute and Department of Electrophysics, National Chiao Tung University, Hsinchu 30010, Taiwan
[e] Advanced Lithium Electrochemistry Co., Ltd., Taoyuan 33048, Taiwan

## HIGHLIGHTS

- *In-situ* neutron powder diffraction was used to study a commercial lithium ion battery.
- The phenomenon of delayed phase transition was not observed in vanadium-added $LiFePO_4$.
- The structural changes of lithium-intercalated graphite are reported.

## GRAPHICAL ABSTRACT

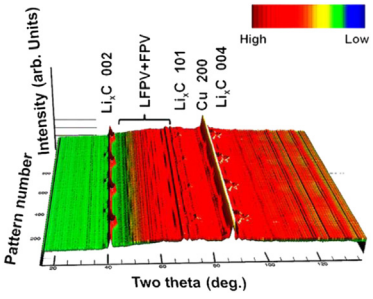


## ARTICLE INFO

*Article history:*
Received 1 October 2012
Received in revised form
24 February 2013
Accepted 25 February 2013
Available online 6 March 2013

*Keywords:*
Lithium-ion battery
Vanadium-addition
Lithium iron phosphate
Neutron powder diffraction
*In-situ* experimentation

## ABSTRACT

*In-situ* neutron powder diffraction was employed to investigate the structural evolution of the electrode materials in a commercial lithium-ion battery used for electric buses in Taiwan. The battery, containing a vanadium-added $LiFePO_4$ cathode, does not exhibit a delayed phase transition between $LiFePO_4$ (triphylite) and $FePO_4$ (heterosite) suggesting that the delayed phase transition can be suppressed through the use of vanadium-added $LiFePO_4$ cathodes, which also enhances the capacity and prolongs the cycle life of these batteries. Furthermore, we characterize the readily reversible structural change of the anode ($Li_xC_6$ where $0 < x \leqq 1$) and correlate this to battery voltage.



## 1. Introduction

Phase transitions of electrode materials occur as Li ions are inserted and extracted from both the cathode and the anode within a lithium-ion battery (LIB) during charging and discharging.

* Corresponding author. Tel.: +886 3 5780281x6405; fax: +886 3 5783805.
*E-mail addresses:* su.huichia@nsrrc.org.tw, train2827@gmail.com (H.-C. Su).
[1] Present address: School of Chemistry, University of New South Wales, Sydney, NSW 2052, Australia.

0378-7753/$ – see front matter © 2013 Elsevier B.V. All rights reserved.
http://dx.doi.org/10.1016/j.jpowsour.2013.02.074

Previous work shows that an understanding of the phase transitions [1–4] is crucial to progressing research aimed at prolonging LIB cycle life and enhancing the LIB rate-capability. Currently, most commercial electrode materials are based on layered rock-salt type crystal structures, composed of Li and transition metal oxides, such as $LiMnO_2$, $LiCoO_2$, … *etc.* for cathodes [5], and graphitic carbon or $LiTiO_x$ for anodes [6]. For application in electric vehicles [7,8], the olivine-type $LiFePO_4$ (LFP) cathode-based LIB is the most promising commercial battery. This is because LFP shows superior safety characteristics relative to other cathode materials. In this work, we study the phase changes of the cathode and the anode of a commercial battery used in electric buses. The cathode material is based on LFP and the anode is made of graphite. Since we are investigating a LIB with a thickness greater than 8 mm which includes several layers of cathodes, anodes, separators, and interconnects, X-rays cannot easily penetrate the LIB pack. Additionally, X-rays are also relatively insensitive to the low-Z elements such as carbon and lithium. Therefore, in this study we take an unmodified bus battery and probe the structural evolution of the electrode materials during conventional battery use by *in-situ* neutron powder diffraction (NPD).

For a LFP battery, Padhi et al. reported a reversible theoretical specific capacity of 170 mAh $g^{-1}$ [9] and a flat potential plateau at 3.4 V *versus* $Li/Li^+$. However, the rate capability is restricted by the intrinsically low electronic conductivity and poor ionic transport properties exhibited by pristine LFP. In order to achieve better performance for electric bus applications, the electrochemical properties need to be improved, especially at the higher C-rates (>5 C). Supervalent-cation addition in the LFP cathode material is a viable method to improve the performance of a LFP cathode [10–13]. Vanadium has been shown to readily substitute into LFP [14,15]. Evidence of vanadium enhanced capacity in LIBs was found by Omenya et al. [16], however, this approach features the addition of relatively high amounts of vanadium and their results show no phase segregation. A distinct peak shift in the X-ray diffraction of the V-added $LiFePO_4$, relative to pure $LiFePO_4$, was also noted. In the present work, we employ a different fabrication process (large-scale manufacturing to optimize performance and minimize cost), and obtain slightly different results, particularly regarding the small amount of V-addition required to improve commercial performance. In this work, the cathode material is vanadium-added LFP and is denoted LFPV. For this system, previous work [17] showed that the capacity and conductivity of LFPV is improved relative to the pristine LFP by 14% and by a factor of 40, respectively. Reliable and reproducible capacity, including relatively small capacity changes at high current, with continuous cycling is also demonstrated, and a less than 10% capacity reduction upon cycling at 20 C relative to 0.1 C. These results are seemingly different to other reports [18–21]. Therefore, a detailed time-dependent study of the LFPV cathode material is carried out to provide further insight into the consequences of the vanadium addition. In particular, a non-destructive real-time study of the relationship between the electrode's structural response and the battery performance in a full-scale commercial LIB is required and directly relevant to practical applications.

Previous X-ray-based reports [2,22,23], found evidence of a delayed phase transition, which is a phenomenon related to the non-synchronization between the phase evolution (phase fraction) and the percentage of Li-ions transferred during electrochemical cycles. For example, the phase fractions of LFP (triphylite) and FP (heterosite) under low charging and discharging currents are expected to undergo a linearly-varying relation at room temperature. However, the phase fractions lag behind the amount of Li-ions inserted or extracted, as calculated electrochemically. For practical applications, an understanding of the mechanism of the delayed phase transition in LFPV as a function of the battery state-of-charge is needed. The delayed phase transition is important because it may be the key to understanding the cycling life-time of LIBs, especially at high C-rates.

On the anode side, although new emerging materials are being developed [6], graphite is still the most popular commercial LIB material, because of its low cost and high capacity [24]. However, the graphite anode still features several problems, such as the formation of solid electrolyte interface (SEI) layers [25]. These problems cause irreversible capacity loss and poor cycling life [26]. An *in-situ* study of the phase evolution of the anode material during electrochemical cycling is important to provide a complete picture of the $Li^+$ transfer that occurs during battery use.

## 2. Experimental

The commercial LIB featuring a nominal capacity of 10 Ah with dimensions, 8.2 mm thick × 128 mm wide × 155 mm high, were obtained from Advanced Lithium Electrochemistry Co. Ltd. (ALEEES), Taiwan. The battery consists of a graphite anode, $LiPF_6$ containing electrolyte, and a carbon coated LFPV cathode. The information provided by the manufacturer states 1% vanadium is added to form LPFV, with the cathode made using a mixture of LPFV and polyvinyl difluoride (PVDF) binder coated onto aluminum foil and containing 75.83 g of the active material. The graphite anode paste is coated onto copper foil with an active material mass of 40.45 g. Copper and aluminum act as current collectors. The electrolyte consists of $LiPF_6$ in a mixture of ethylene carbonate (EC) and dimethyl carbonate (DMC). The *in-situ* neutron powder diffraction (NPD) experiment was performed on Wombat, the high-intensity powder diffractometer at the OPAL reactor facility in the Australian Nuclear Science and Technology Organisation (ANSTO) [27]. The NPD patterns were measured using a wavelength of 2.4086 Å which was determined using the NIST $Al_2O_3$ SRM 676 standard. Similar *in-situ* experiments have been conducted on this instrument in the past [28–33]. Here, we use a relatively large battery for these experiments and the neutron beam only impinges on 40 × 20 mm of the whole battery. In order to collect the NPD patterns, the neutron beam was aligned centrally with respect to the height of the battery and one edge of the battery was exposed to the neutron beam. The angle between the battery and incoming neutron beam was adjusted to maximize the signal from the electrodes. During the data collection, the battery was operated between 2.0 and 3.8 V at a constant current (CC) of 1 A which corresponds to 0.1 C. NPD patterns were collected at room temperature in the $2\theta$ range from 15° to 135° with an exposure time of 5 min per pattern. NPD data is collected using Wombat's continuous 2D detector and each pattern is normalized with respect to incident beam intensity. Single peak fits were undertaken using the Large Array Manipulation Program (LAMP) [34] with a Gaussian peak-shape and an adjustable flat background.

## 3. Results and discussion

Fig. 1 shows the *in-situ* 3-dimensional NPD patterns of the as-made LIB during the 1st to 4th charging and discharging cycles between 2.0 and 3.8 V at 0.1 C. The vertical axis going into the page in Fig. 1(a) is time, where each pattern represents 5 min. The time progression correlates to the charging and discharging cycles as shown in Fig. 1(b). This battery was found to have a specific capacity of about 11.3 Ah. From Fig. 1(a), the structural transformation between triphylite and heterosite at the cathode can be observed and the lattice contraction and expansion as a result of lithium fluctuations in $Li_xC_6$ at the anode can be seen via the 002 graphite peak at $2\theta \sim 42°$. Each NPD pattern in Fig. 1(a) can be represented as shown

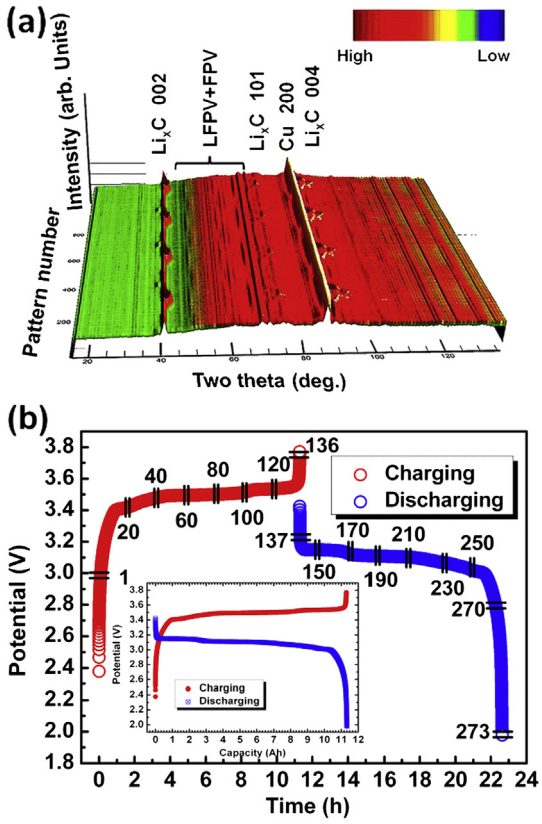


**Fig. 1.** (a) *In-situ* NPD patterns collected during 4 charging/discharging cycles of an as-made LIB under 0.1 C at room temperature. The inset shows the color intensity scale and the numbers marked beside the patterns correspond to the NPD pattern numbers. (b) The charging/discharging curves of the same cell between 2.0 V and 3.8 V at 0.1 C.

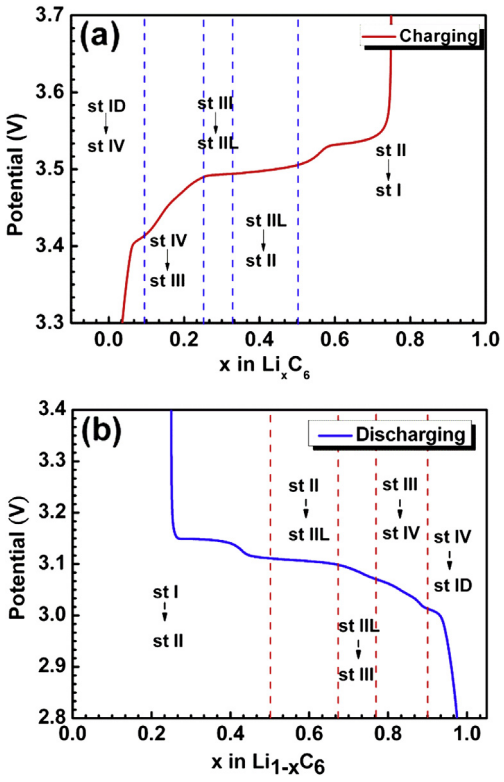


**Fig. 3.** The electrochemical response during (a) charging and (b) discharging of a commercial battery using a current corresponding to 0.1 C at room temperature. The sequential phases identified during the electrochemical cycles include: dilute stage I (st ID), stage IV (st IV), stage III (st III), liquid-type stage II (st IIL), stage II (st II), and stage I (st I). Note that approximately 75% of lithium is cycled during the battery operation as shown in the *x*-axis.

in Fig. 2. Although the background in the NPD pattern is high due to the use of hydrogenated electrolyte, the signal-to-noise ratio is sufficient for meaningful data interpretation and analysis. In addition, since the sample geometry is non-annular, the differences in neutron path-lengths may affect the background in the NPD pattern. We discuss our results from the diffraction data for the anode and cathode in separate sections below.

### 3.1. Anode

Lithium ions are inserted into and extracted from the graphite lattice during the charging and discharging processes, respectively. Fig. 3 shows the electrochemical response of the battery along with

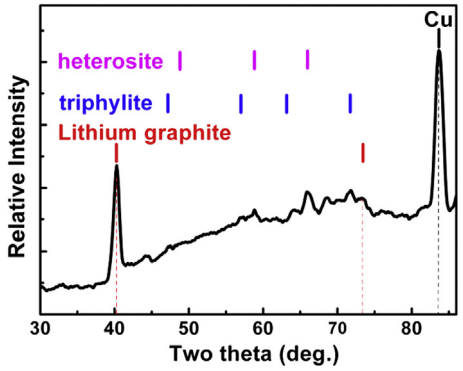


**Fig. 2.** A typical NPD pattern of the commercial LIB collected with identified phases labeled.

the identified charge products: Dilute stage I, stage VI (whose composition is not well defined), stage III ($LiC_{24}$), liquid-type stage II ($LiC_{18}$), stage II ($LiC_{12}$), and stage I ($LiC_6$) [35].

With increasing Li concentration, the $Li_xC_6$ intercalation occurs in stages, where the stage number $n$ contains $n$ empty layers between each Li-filled layer [36]. For a range of $x$ in $Li_xC_6$ from 0 to 1, the theoretical calculation of the capacity of graphite is 15.05 Ah (372 mAh $g^{-1}$ [37] × 40.45 g), which is greater than the specific capacity of 11.3 Ah that we obtained during cycling. This is related to the ratio of active cathode and anode materials and the amount of lithium that can be extracted/inserted from the electrodes at the C-rate used. *In-situ* NPD data also illustrate this, as not all the $Li_xC_6$ anode is converted to the fully lithiated $LiC_6$ compound during charge. Approximately 75% lithium insertion/extraction occurs in the $Li_xC_6$ anode. In order to approximate the $x$ values in $Li_xC_6$ we assume $x = 0$ at 0 Ah and $x = 1$ at 15.05 Ah with the $x$ values increasing linearly with respect to electrochemical cycling process. Fig. 4 shows the evolution of the *in-situ* NPD patterns during charging (Fig. 4(a)) and discharging (Fig. 4(b)). The numbers marked beside the NPD diffraction patterns are the pattern numbers (time evolution). The diffraction pattern marked "1" is collected at the beginning of charging process with the numbers increasing as charging proceeds. Changes of the $Li_xC_6$ ($0 < x < 1$) 002 and $LiC_6$ 001 reflections were observed. At the initial stage of charging, lithium ions occupy the available sites between the graphite layers, dilute stage I, causing the $2\theta$ value of the 002 reflection to shift to slightly lower angles (larger $d$-spacings). During charging, the anode material is a compound of nominal composition $LiC_{18}$, the liquid-type stage II product, whose 002 reflection shifts to approach $2\theta = 40.2^\circ$ at $x \sim 0.32$ in $Li_xC_6$. At this

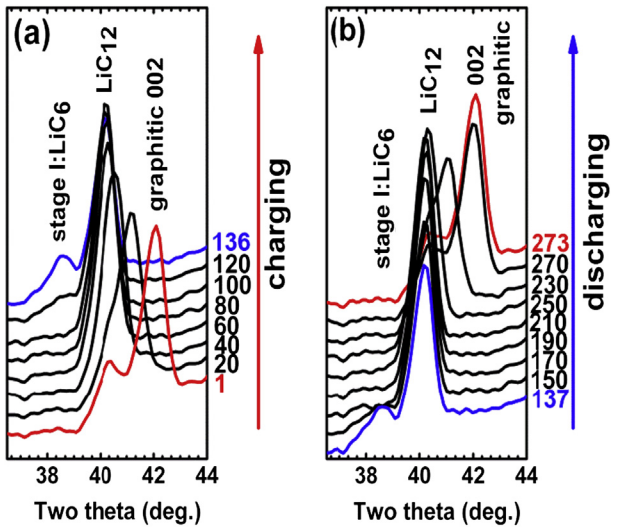


**Fig. 4.** *In-situ* NPD patterns of the graphite anode during (a) charging and (b) discharging at 0.1 C. The numbers marked beside the NPD diffraction patterns are the pattern numbers. Each pattern was collected for 5 min.

point, lithium atoms feature no long-range ordering within the layers [38]. After ~50% charging, $LiC_{12}$ ($Li_{0.5}C_6$) forms with the lithium arranging in a highly ordered hexagonal structure. As $x$ (in $Li_xC_6$) increases to ~0.61, the stage I ($LiC_6$) 001 reflection is observed and the stage II ($LiC_{12}$) 002 reflection does not shift continuously in $2\theta$ value toward lower angles. Instead, the reflection abruptly transitions or "jumps" from a position corresponding to $LiC_{12}$ to one corresponding to $LiC_6$, indicating a two-phase reaction. As $x$ in $Li_xC_6$ increases from 0.61 to the end of charge, the intensity of the $LiC_{12}$ 002 reflection decreases while the intensity of the $LiC_6$ 001 reflection increases, as similar to previous reports [29,39]. The $LiC_6$ phase is approximately 26.3% of the final anode composition at the charged state. Fig. 4(b) shows that the changes in the diffraction peaks vary in the opposite direction as the battery is discharged which corresponds to the average interlayer spacing shifting back toward the initial graphite composition of the anode. This result at the anode shows a reversible process during electrochemical cycling.

### 3.2. Cathode

Typical structural transformations between triphylite and heterosite phases at the cathode are presented in Fig. 5. Here, the selected NPD pattern numbers correspond to those shown in Fig. 1(b) alongside the charging and discharging curves. The lithium content, $y$ in $Li_{1-y}FePO_4V$ was calculated by assuming $y = 0$ at 0 Ah and $y = 1$ at 11.3 Ah with a linear combination of these two phases upon electrochemical cycling.

During the charging process, the amount of the triphylite phase reduces and the heterosite phase increases as expected. This phase evolution indicates the extraction of lithium ions from the triphylite phase. In the literature [2,22,23], reflections of pristine LFP cathodes can be indexed to triphylite and heterosite phases up to ~60% state-of-charge during the charging cycle, even at 0.1 C at room temperature. During the discharging process, a substantial amount of heterosite remains in the electrode until near the end of discharging and then rapidly transforms to triphylite. Studies by Wang et al. [22] using *ex-situ* soft X-ray absorption at Fe $L_{II,III}$ edges show that the Li content in the bulk cathode material changes more slowly than that calculated from the charging rates, but at the cathode surface, the Li content is linearly correlated to the charging

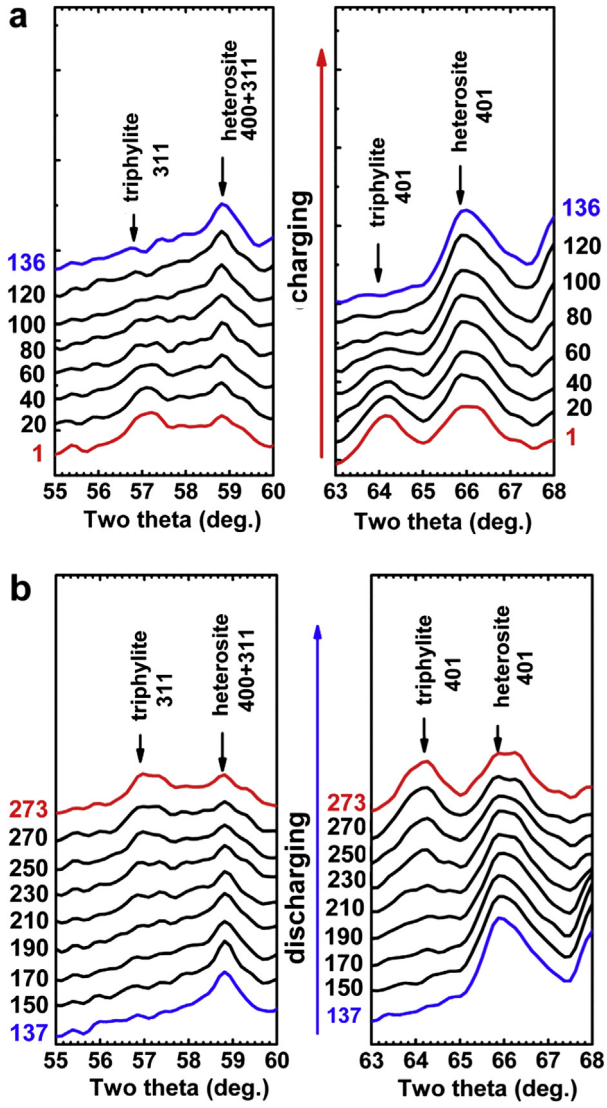


**Fig. 5.** *In-situ* NPD patterns of triphylite (LFPV) and heterosite (FPV) during the first (a) charging and (b) discharging cycle. The number alongside the patterns is the NPD pattern number marked in the charging and discharging curves of Fig. 1(b).

rate. These results are characteristic of the delayed phase transition phenomenon. However, in our *in-situ* NPD data, the delayed phase transition was not observed. The percentage of triphylite and heterosite at each $y$ value in $Li_{1-y}FePO_4V$ (charging cycle) and $Li_yFePO_4V$ (discharging cycle) are shown in Fig. 6, as derived from single-peak fits of the triphylite and heterosite 401 reflections. Fig. 6 shows an almost linear behavior of the phase composition of the cathode (dashed lines), indicating that the structural changes in $Li_{1-y}FePO_4V$ ($Li_yFePO_4V$) are effectively synchronized with the electrochemical cycling process (voltage profile).

A possible explanation of the suppressed delayed phase phenomenon may be the vanadium in our sample. In order to quantify the influence of V-addition into LFP on the delayed reaction mechanism we undertook *in-situ* X-ray powder diffraction measurements on pristine and V-added LFP cells (Figure S1 in the Electronic Supplementary Information). We find a significant suppression of the delay in the phase transition, by about 20%, when a vanadium-added LFP cathode is used. This result indicates that vanadium is playing a part in the kinetics of the charge/discharge processes. According to the suggestions from Chang et al. [2], the delayed phase transition results from the slow nucleation kinetics

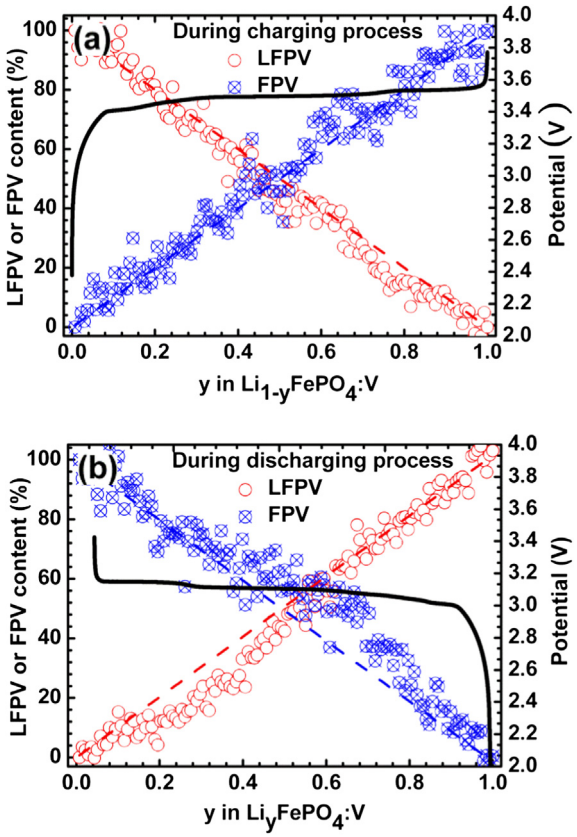


**Fig. 6.** Triphylite (LFPV) and heterosite (FPV) contents calculated from *in- situ* NPD patterns as a function of delithiation or lithiation ($y$ in $Li_{1-y}FPV$ or $Li_yFPV$) during the (a) charging and (b) discharging cycle.

of the resulting phase and disturbing the linear conversion of triphylite to heterosite during the charging–discharging cycling. Our cathode contains vanadium-added LFP, and therefore may have faster nucleation kinetics (of the delithiated or lithated phase) than LFP alone, resulting in the synchronization of the phase transition. This supports our previous work [17] that shows vanadium incorporation into the olivine structure can induce lithium vacancies, which may improve nucleation kinetics and hence contribute to the suppression of the delayed phase transition.

Previous studies of the delayed phase transition [2,22,23] use *in-situ* X-ray experiments with a half-cell sample to overcome the small penetration depth of X-rays. Furthermore, the X-ray beam is generally less than 0.5 mm, much smaller than the size of the electrode. Without a correction for the non-uniformity of the sample, the specific location of X-ray beam in conjunction with its small penetration depth mean that the details concerning the delayed phase reaction are location-biased and not representative of the bulk cathode behavior. Additionally, Christian Masquelier suggested in a recent unpublished finding, that the delayed phase transformation might arise from insufficient contacts between components in the LIB during *in-situ* X-ray powder diffraction experiments. The additional windows and spacers used to allow the X-ray beam to access the cathode in *in-situ* X-ray diffraction experiments may result in a loss of contact at these areas and, consequently, slower transitions. The innovative use of X-ray fluorescence was used to show that this is the case, where the transition was found to be slower in regions of less contact. In the present work, the problems of sample non-uniformity and poor contacts are eliminated by the highly-penetrating neutron beam and relatively larger area of illumination compared with X-ray beam measurements. The resulting data are from several layers of anode and cathode and therefore represent the average electrode structure. To make a meaningful comparison between different experiments published on the phase delay issue, factors such as charge/discharge rates, type of electrolytes, cycling history of the battery, operating temperature and voltage ranges, and vanadium ordering must be comparable.

## 4. Conclusions

Structural phase transitions of a vanadium-added LFP cathode and a graphite anode in a commercial Li-battery were investigated by *in-situ* NPD. At the anode, we characterize the phase evolution of $Li_xC_6$ for $0 < x \leqq 1$. At the cathode, a delayed phase transition was not observed, which we show to be, at least in part, a result of the vanadium-addition.

## Acknowledgments

The authors would like to acknowledge the financial support for this work from the Advanced Lithium Electrochemical Co., Ltd. (ALEEES), and the traveling budget provided by National Synchrotron Radiation Research Center (NSRRC) for the neutron experiment.

## Appendix A. Supplementary materials

Supplementary materials related to this article can be found at http://dx.doi.org/10.1016/j.jpowsour.2013.02.074.

## References

[1] J.L. Allen, T.R. Jow, J. Wolfenstine, J. Solid State Electrochem. 12 (2008) 1031–1033.
[2] H.H. Chang, C.C. Chang, H.C. Wu, M.H. Yang, H.S. Sheu, N.L. Wu, Electrochem. Commun. 10 (2008) 335–339.
[3] J.L. Allen, T.R. Jow, J. Wolfenstine, Chem. Mater. 19 (2007) 2108–2111.
[4] Y.F. Reynier, R. Yazami, B. Fultz, J. Electrochem. Soc. 151 (2004) A422–A426.
[5] M.S. Whittingham, Chem. Rev. 104 (2004) 4271–4301.
[6] F. Kenjiro, I. Keita, I. Shigeru, Sci. Technol. Adv. Mater. 12 (2011) 054203.
[7] A.F. Burke, M. Miller, The UC Davis Emerging Lithium Battery Test Project, Institute of Transportation Studies, University of California, Davis, Research Report UCD-ITS-RR-09-18.
[8] S.B. Peterson, J.F. Whitacre, J. Apt, J. Power Sources 195 (2010) 2377–2384.
[9] A.K. Padhi, K.S. Nanjundaswamy, J.B. Goodenough, J. Electrochem. Soc. 7 (1997) 1188–1194.
[10] A. Goni, L. Lezama, A. Pujana, A.M.I. Arriortua, T. Rojo, Int. J. Inorg. Mater. 3 (2001) 937–942.
[11] A. Yamada, Y. Takei, H. Koizumi, N. Sonoyama, R. Kanno, K. Itoh, M. Yonemura, T. Kamiyama, Chem. Mater. 18 (2006) 804–813.
[12] M.S. Islam, D.J. Driscoll, C.A.J. Fisher, P.R. Slater, Chem. Mater. 17 (2005) 5085–5092.
[13] M. Wagemaker, B.L. Ellis, Chem. Mater. 20 (2008) 6313–6315.
[14] J. Hong, C.S. Wang, X. Chen, S. Upreti, M.S. Whittingham, Electrochem. Solid State Lett. 12 (2009) A33–A38.
[15] Y. Wen, L. Zeng, Z. Tong, L. Nong, W. Wei, J. Alloys Compd. 416 (2006) 206–208.
[16] F. Omenya, N.A. Chernova, S. Upreti, P.Y. Zavalij, K.W. Nam, X.Q. Yang, M.S. Whittingham, Chem. Mater. 23 (2011) 4733–4740.
[17] C.Y. Chiang, H.C. Su, P.J. Wu, H. Liu, C.W. Hu, N. Sharma, V.K. Peterson, H.W. Hsieh, Y.F. Lin, W.C. Chou, C.H. Lee, J.F. Lee, B.Y. Shew, J. Phys. Chem. C 116 (2012) 24424–24429.
[18] T. Zhao, W. Xu, Q. Ye, J. Cheng, H. Zhao, Z. Wu, D. Xia, W. Chu, J. Synchrotron Radiat. 17 (2010) 584–589.
[19] L. Wang, Z. Li, H. Xu, K. Zhang, J. Phys. Chem. C 112 (2008) 308–312.
[20] M.R. Yang, W.H. Ke, S.H. Wu, J. Power Sources 165 (2007) 646–650.
[21] N. Hua, C.Y. Wang, X.Y. Kang, T. Wumair, Y. Han, J. Alloys Compd. 503 (2010) 204–208.
[22] X.J. Wang, C. Jaye, K.W. Nam, B. Zhang, H.Y. Chen, J. Bai, H. Li, X. Huang, D.A. Fischer, X.Q. Yang, J. Mater. Chem. 21 (2011) 11406–11411.
[23] H.C. Shin, K.Y. Chung, W.S. Min, D.J. Byun, H. Jang, B.W. Cho, Electrochem. Commun. 10 (2008) 536–540.
[24] Z.X. Shu, R.S. McMillan, J.J. Murray, I.J. Davidson, J. Electrochem. Soc. 143 (1996) 2230–2235.
[25] H.L. Zhang, F. Li, C. Liu, J. Tan, H.M. Cheng, J. Phys. Chem. B 109 (2005) 22205–22211.

[26] D. Goers, M. Holzapfel, W. Scheifele, E. Lehmann, P. Vontobel, P. Novák, J. Power Sources 130 (2004) 221–226.
[27] A.J. Studer, M.E. Hagen, T.J. Noakes, Phys. B 385–386 (2006) 1013–1015.
[28] N. Sharma, X. Guo, G. Du, Z. Guo, J. Wang, Z. Wang, V.K. Peterson, J. Am. Chem. Soc. 134 (2012) 7867–7873.
[29] N. Sharma, V.K. Peterson, M.M. Elcombe, M. Avdeev, A.J. Studer, N. Blagojevic, R. Yusoff, N. Kamarulzaman, J. Power Sources 195 (2010) 8258–8266.
[30] N. Sharma, M.V. Reddy, G. Du, S. Adams, G.V. Subba Rao, B.V.R. Chowdari, Z. Guo, V.K. Peterson, J. Phys. Chem. C 115 (2011) 21473–21480.
[31] G. Du, N. Sharma, V.K. Peterson, J. Kimpton, Z. Guo, Adv. Funct. Mater. 21 (2011) 3990–3997.
[32] N. Sharma, G. Du, A.J. Studer, Z. Guo, V.K. Peterson, Solid State Ionics 199–200 (2011) 37–43.
[33] N. Sharma, V.K. Peterson, J. Solid State Electrochem. 16 (2012) 1849–1856.
[34] D. Richard, M. Ferrand, G.J. Kearley, J. Neutron Res. 4 (1996) 33–39.
[35] S. Flandroisa, B. Simon, Carbon 37 (1999) 165–180.
[36] K. Persson, Y. Hinuma, Y.S. Meng, A. Van der Ven, G. Ceder, Phys. Rev. B 82 (2010) 125416.
[37] J.M. Tarascon, M. Armand, Nature 414 (2001) 359–367.
[38] R. Yazami, Y. Reynier, J. Power Sources 153 (2006) 312–318.
[39] A. Saito, N. Takami, T. Ohsaki, Solid State Ionics 80 (1995) 291–298.